IAI Journals.ASM.org

Distinct Compartmentalization of NF-κB Activity in Crypt and Crypt-Denuded Lamina Propria Precedes and Accompanies Hyperplasia and/or Colitis following Bacterial Infection

Parthasarathy Chandrakesan,[a] Ishfaq Ahmed,[a] Anisha Chinthalapally,[a] Pomila Singh,[b] Shanjana Awasthi,[c] Shrikant Anant,[d] and Shahid Umar[d]

Department of Internal Medicine, Division of Digestive Diseases and Nutrition,[a] and Department of Pharmaceutical Sciences,[c] University of Oklahoma Health Sciences Center, Oklahoma City, Oklahoma, USA; Department of Neuroscience and Cell Biology, University of Texas Medical Branch, Galveston, Texas, USA[b]; and Department of Molecular and Integrative Physiology, University of Kansas Medical Center, Kansas City, Kansas, USA[d]

Citrobacter rodentium **induces transmissible murine colonic hyperplasia (TMCH) and variable degrees of inflammation and necrosis depending upon the genetic background. Utilizing *C. rodentium*-induced TMCH in C3H/HeNHsd inbred mice, we observed significant crypt hyperplasia on days 3 and 7 preceding active colitis. NF-κB activity in the crypt-denuded lamina propria (CLP) increased within 24 h postinfection, followed by its activation in the crypts at day 3, which peaked by day 7. Increases in interleukin-α1 (IL-1α), IL-12(p40), and macrophage inflammatory protein 1α (MIP-1α) paralleled NF-κB activation, while increases in IL-1α/β, IL-6/IL-12(p40)/granulocyte colony-stimulating factor (G-CSF)/keratinocyte-derived chemokine (KC)/monocyte chemotactic protein 1 (MCP-1), and MIP-1α followed NF-κB activation leading to significant recruitment of neutrophils to the colonic mucosa and increased colonic myeloperoxidase (MPO) activity. Phosphorylation of the crypt cellular and nuclear p65 subunit at serines 276 and 536 led to functional NF-κB activation that facilitated expression of its downstream target, CXCL-1/KC, during TMCH. Distinct compartmentalization of phosphorylated extracellular signal-regulated kinase 1 and 2 ([ERK1/2] Thr^{180}/Tyr^{182}) and p38 (Thr^{202}/Tyr^{204}) in the CLP preceded increases in the crypts. Inhibition of ERK1/2 and p38 suppressed NF-κB activity in both crypts and the CLP. Dietary administration of 6% pectin or 4% curcumin in *C. rodentium*-infected mice also inhibited NF-κB activity and blocked CD3, F4/80, IL-1α/β, G-CSF/MCP-1/KC, and MPO activity in the CLP while not affecting NF-κB activity in the crypts. Thus, distinct compartmentalization of NF-κB activity in the crypts and the CLP regulates crypt hyperplasia and/or colitis, and dietary intervention may be a novel strategy to modulate NF-κB-dependent protective immunity to facilitate crypt regeneration following *C. rodentium*-induced pathogenesis.**

The intestinal epithelium provides a physical barrier that separates trillions of commensal bacteria in the intestinal lumen from the underlying lamina propria and deeper intestinal layers. In the colon, the epithelial cell homeostasis is tightly regulated; minor perturbations can lead to colitis or neoplasia (25). The human intestine is the site of an extraordinarily complex and dynamic environmentally transmitted interaction of the local immune system with nutrients and microbial products (19). A network of regulatory genes links signals provided by luminal antigens (Ags) to immune and inflammatory cells. In this context the regulation of resident intestinal macrophages by the recognition of conserved pathogen-associated molecular patterns by Toll-like receptors (TLRs) and intracellular sensors such as nucleotide-binding oligomerization domains is critical for understanding the homeostasis of gut-associated immunity. Deciphering the pathways involved in the regulation of intestinal macrophages promises to provide new host targets for treating diseases such as inflammatory bowel disease (IBD) in which a dysregulation of innate immunity plays a role (28).

Nuclear factor kappa B (NF-κB) is a family of ubiquitously expressed transcription factors that are widely believed to trigger both the onset and the resolution of inflammation. NF-κB also governs the expression of genes encoding proteins essential in control of stress response, maintenance of intercellular communications, and regulation of cellular proliferation and apoptosis. NF-κB is sequestered in the cytoplasm by its inhibitor, IκB, which in response to inflammatory stimuli is phosphorylated and targeted for degradation by the proteasome (9). Phosphorylation of the p65 subunit in one of two of its transactivation domains (39) has been shown to be essential for NF-κB-dependent transcriptional activation. The role of the NF-κB pathway in intestinal epithelial cells, as reported recently using IκB kinase (IKK) subunit knockout mice (10, 17), is critical for intestinal immune homeostasis. However, it is not clear how distinct compartmentalization of NF-κB activity in the epithelium and cells of the lamina propria following infection by enteric pathogens affects hyperplasia and/or colitis. We therefore hypothesized that distinct compartmentalization of NF-κB activity in the crypts and crypt-denuded lamina propria (CLP) will regulate hyperplasia and/or colitis following bacterial infection. This hypothesis was tested in an *in vivo* model of hyperproliferation/hyperplasia of the colonic crypts.

Citrobacter rodentium is a natural noninvasive bacterial pathogen which infects the distal colon of mice. It uses the same molecular mechanisms of type III secretion as human enteropathogenic

Received 27 October 2011 **Accepted** 15 November 2011
Published ahead of print 5 December 2011
Editor: S. M. Payne
Address correspondence to Shahid Umar, sumar@kumc.edu.
Supplemental material for this article may be found at http://iai.asm.org/.

doi:10.1128/IAI.06101-11

and enterohemorrhagic *Escherichia coli* (EPEC and EHEC, respectively) to colonize the epithelial cells of the gut. Given the difficulty of infecting laboratory mice with these diarrhea-causing *E. coli* pathogens, infection with *C. rodentium* provides a robust *in vivo* model system to study host-bacterial pathogen interactions in real time (7, 21). Transmissible murine colonic hyperplasia (TMCH) caused by *C. rodentium* is characterized by significant hyperplasia, accompanied by expansion of the proliferative compartment throughout the longitudinal crypt axis (26). Hyperplasia is characteristic of gut inflammation in inflammatory bowel disease and celiac disease as well. Because hyperplasia is observed in infectious and noninfectious intestinal inflammation, it has been predicted to be secondary to the production of inflammatory cytokines, which can act as growth factors for specific cell types. Interestingly, unlike human conditions, TMCH is self-limiting, leading to disease resolution and protective immunity. In contrast to outbred NIH/Swiss mice that develop colonic hyperplasia with little inflammation, inbred strains of mice, including C3H/HeNSd (C3H), FVB/N, and C57BL/6, develop colitis when infected with *C. rodentium* (2, 8, 36).

Utilizing the *C. rodentium*-infected NIH/Swiss outbred mice, which do not exhibit an inflammatory axis, we showed previously that NF-κB activation in the colonic crypts followed both the canonical and atypical pathways (11, 38). Moreover, sustained activation was observed despite a lack of bacterial attachment to the colonic mucosa beyond peak hyperplasia (12 days after *C. rodentium* infection) (11, 38). We have also shown that a pectin diet inhibits increases in both β-catenin levels and NF-κB activity, thereby abrogating hyperplasia of colonic crypts in response to *C. rodentium* infection in the NIH/Swiss mice (29, 11). In the current study, we systematically analyzed distinct compartmentalization of NF-κB activity in the epithelium and cells of the lamina propria constituting the stroma following *C. rodentium* infection and investigated how signaling via extracellular signal-regulated kinase (ERK) and p38 mitogen-activated protein kinases (MAPKs) modulates functional NF-κB activity in various cell types in the distal colons of C3H inbred mice. We also examined how dietary intervention modulates NF-κB activity *in vivo*, thereby affecting epithelial regeneration following a pathogenic insult.

MATERIALS AND METHODS

TMCH, inhibitor studies, and diets. This study was carried out in strict accordance with the recommendations in the Guide for the Care and Use of Laboratory Animals of the National Institutes of Health. All animal work was approved by the University of Oklahoma Institutional Animal Care and Use Committee. TMCH was induced in 5- to 6-week old *Helicobacter*-free C3H/HeNHsd mice (Harlan Laboratories, Inc., Indianapolis, IN) by oral inoculation with a 16-h culture of *C. rodentium* (26, 29–35, 38). Age- and sex-matched control mice received sterile culture medium only. To investigate the role of ERK1 and ERK2 (ERK1/2) and p38 MAPKs in the regulation of NF-κB activity *in vivo*, highly selective ERK1/2 (PD98059 [PD]) and p38 (SB203580 [SB]) inhibitors were used. PD98059 and SB203580 (5 mg/kg of body weight) or vehicle (1% dimethyl sulfoxide [DMSO]) was administered intraperitoneally for 5 days starting at 2 days postinfection with *C. rodentium*. At 2 h following the last injection, mice were euthanized, and distal colons were removed. For dietary intervention, mice were randomized to receive either a control AIN-93 diet (29) or a 6% pectin, synthesized by Harlan Teklad (Madison, WI), and 4% curcumin diet. Animals were euthanized at 1, 3, 5, and 7 days postinfection, and distal colons were removed. Animals under various dietary regimens were killed at 9 days postinfection, and their colons were harvested. Histology scoring (0 to 4) to determine the effect of dietary intervention on inflammation and/or colitis was done by blindly assessing the degree of lamina propria mononuclear cell (LPMC) infiltration, crypt hyperplasia, goblet cell depletion, and architectural distortion in hematoxylin and eosin (H&E)-stained sections as described by Berg et al. (3). A score of 0 to 1 was regarded as no inflammation, 1 to 2 indicated mild inflammation, 2 to 3 indicated moderate inflammation, and 3 to 4 indicated severe inflammation. Distal colonic crypts or crypt-denuded lamina propria from various groups were prepared for biochemical assays as described previously (26, 29–35, 38).

Cell culture, DNA binding assay, and NF-κB reporter activity. Crypt-denuded mucosal tissues after crypt removal were chopped into small pieces, washed with medium, and plated for monolayer formation at 37°C. After two passages, the stromal cells were trypsinized and plated into 96-well plates for 24 h. To start the coculture, YAMC cells, maintained at 33°C, were layered onto the stromal cells at a 1:1 ratio and incubated at 37°C. At 24 h after the coculture, cells were infected with *C. rodentium* at a multiplicity of infection (MOI) of 90 for 3 h. Cells were then washed to remove bacteria and incubated at 37°C for 48 h. NF-κB activity was measured using a TransAM p65 NF-κB Chemi Transcription Factor assay kit from Active Motif (Carlsbad, CA). Both YAMC and JAWSII dendritic cell (DC) lines were maintained as described previously (11). To measure the reporter activity, both YAMC and JAWSII cells were transiently transfected with an NF-κB–luciferase reporter plasmid [pGL4.32(luc2P/NF-κB-RE/hygro)] from Promega (Madison, WI) using LipoD293 transfection reagent (SignaGen Laboratories, Ijamsville, MD). At 36 h after the transfection, cells were infected with *C. rodentium* at an MOI of 90 for 3 h. Cells were then washed to remove bacteria and incubated at 37°C for 48 h, and the luciferase activity was measured using a Bright-Glo luciferase assay system (Promega, Madison, WI).

RNA isolation and real-time quantitative reverse transcription-PCR (RT-PCR). Total RNA was extracted from uninfected control crypts and crypts from days 3 to 7 or from crypts isolated from the distal colons of C3H mice treated with vehicle or PD98059 and SB203580 using an RNA Isolation Kit from Qiagen. To measure expression levels of CXCL-1/keratinocyte-derived chemokine (KC) in the colonic crypts or CLP, total RNA samples were subjected to real-time PCR by SYBR chemistry (SYBR green I; Molecular Probes, Eugene, OR) using gene-specific primers and Jumpstart *Taq* DNA polymerase (Sigma-Aldrich, St. Louis, MO). The crossing threshold value assessed by real-time PCR was noted for the transcripts and normalized with β-actin mRNA. The changes in mRNA were expressed as fold change relative to control ± the standard error of the mean (SEM).

Western blotting. Cellular or nuclear extracts prepared from crypts or crypt-denuded lamina propria (30 to 100 μg protein/lane) were subjected to SDS-PAGE and electrotransferred to nitrocellulose membrane. The efficiency of electrotransfer was checked by back-staining gels with Coomassie blue and/or by reversible staining of the electrotransferred protein directly on the nitrocellulose membrane with Ponceau S solution. No variability in transfer was noted. Destained membranes were blocked with 5% nonfat dried milk in Tris-buffered saline ([TBS] 20 mm Tris-HCl and 137 mm NaCl [pH 7.5]) for 1 h at room temperature and then overnight at 4°C. Immuno-antigenicity was detected by incubating the membranes for 1 to 2 h with the appropriate primary antibodies (0.5 to 1.0 μg/ml in TBS containing 0.1% Tween 20 [TBS-Tween]) (Sigma). After membranes were washed, they were incubated with horseradish peroxidase (HRP)-conjugated anti-mouse or anti-rabbit secondary antibodies and developed using an ECL detection system (Amersham Corp., Arlington Heights, IL) according to the manufacturer's instructions.

Measurement of colonic cytokines/chemokines. For cytokine/chemokine measurement, distal colons were collected from uninfected and *C. rodentium*-infected C3H mice with or without dietary interventions, washed with saline, and homogenized in phosphate-buffered saline (PBS). Protein concentration was assessed using a detergent-compatible (DC) protein assay kit (Bio-Rad). The cytokine/chemokine concentration in the colonic extracts was measured in triplicate using a Bio-Plex Pro

Mouse Cytokine 23-Plex Assay kit (Bio-Rad, Hercules, CA) according to the manufacturer's protocol.

Measurement of MPO activity. Myeloperoxidase (MPO) activity, an index of neutrophil recruitment, was measured in colon tissue homogenates by a modification of the method of Grisham (15). Briefly, colon homogenate was sonicated in 1% hexadecyltrimethyl-ammonium bromide buffer and subjected to centrifugation at 12,000 revolutions/min at 4°C for 20 min. MPO activity in the homogenates was measured in triplicate using a Fluoro MPO detection kit (Cell Technology, Inc., CA) according to the manufacturer's protocol.

IHC. Immunohistochemistry (IHC) for Ki-67, CD3, F4/80, and p65 phosphorylated at Ser-276 ($p65^{276}$) was performed on 5-μm-thick paraffin-embedded sections from distal colons of uninfected, *C. rodentium*-infected, *C. rodentium*-infected and MAPK inhibitor-treated, and *C. rodentium*-infected and diet-treated mouse distal colons utilizing HRP-labeled polymer conjugated to secondary antibody using an Envision+ System-HRP (diaminobenzidine [DAB]; DakoCytomation, Carpinteria, CA) with microwave accentuation as described previously (11, 29–33). Slides were washed and incubated with 4′,6′-diamidino-2-phenylindole for 5 min at room temperature to stain the nuclei. The visualization was carried out via either fluorescent or light microscopy. Controls included either omission of primary antibody or detection of endogenous IgG staining patterns with goat anti-mouse or anti-rabbit IgG (Calbiochem, San Diego, CA).

RESULTS

Within 7 days following *C. rodentium* infection, there was gross thickening of the distal colon of C3H mice, accompanied by hyperplasia and a 3-fold increase in crypt length (Fig. 1A). In 9-day-postinfection mice, however, we observed significant colitis associated with crypt abscess and necrosis (Fig. 1A). To determine if these increases in crypt length were due to increased proliferation of colonic epithelial cells, we next stained the paraffin-embedded sections for Ki-67. In normally proliferating crypts, only cells at the base exhibited nuclear staining (Fig. 1B). During TMCH, however, there was a gradual increase in Ki-67-positive cells at days 3 and 7 compared to levels in the uninfected control, and the level remained elevated at day 9 (Fig. 1B). These changes correlated well with increased crypt length at day 7 and crypt abscess at day 9 of TMCH (Fig. 1A).

We next determined the kinetics of NF-κB activity in the colonic crypts of C3H mice in response to *C. rodentium* infection. Nuclear NF-κB activity increased within day 1 postinfection, but the activation was much more significant after day 5 of TMCH (Fig. 2A). This coincided with hyperplasia of the colonic crypts. These changes in NF-κB activity also correlated with CXCL-1 mRNA expression as determined by real-time PCR (Fig. 2B). CXCL-1 is a downstream target of NF-κB and a cognate ligand for the CXC-chemokine receptor CXCR-2. We have shown previously that NF-κB activation by *C. rodentium* induces both the canonical pathway involving phosphorylation of cellular IKKα/β and phosphorylation and degradation of IκBα at peak hyperplasia and the pathway of NF-κB activation, which was independent of IκBα degradation (11, 38). In the current study, while we detected presence of IκBα, -β, and -ε and p105 along with IKKα/β in the colonic crypts, the changes observed did not correlate with NF-κB activation (data not shown), suggesting involvement of a complex regulatory mechanism for NF-κB activation in the colonic crypts of C3H mice following *C. rodentium* infection. Since functional NF-κB activation is associated with critical phosphorylation events at consensus phosphorylation sites in the p65 subunit, we instead concentrated on delineating the presence or absence of the phosphorylated subunit in various compartments of the colonic mucosa in order to understand the functional role of NF-κB following a bacterial infection.

We have recently shown that NF-κB activation during both progression and regression phases of hyperplasia in NIH/Swiss mice is associated with phosphorylation and acetylation of the p65 subunit and is independent of IκBα degradation, particularly during regression (11). Utilizing antibodies specific for detecting phosphorylation of the p65 subunit at Ser-276 ($p65^{276}$) and Ser-536 ($p65^{536}$), respectively, we probed both crypt cellular and nuclear extracts during the time course of TMCH. As shown in Fig. 2C, cellular and nuclear levels of $p65^{276}$ and $p65^{536}$ along with total p65 increased significantly at days 5 and 7, thereby correlating with increases in NF-κB activity at these time points (see Fig. 2A). Interestingly, we observed significantly more phosphorylation of p65 at Ser-276 than at Ser-536, particularly in the nuclear fraction relative to total p65, suggesting a relatively more important role for $p65^{276}$ in the functional activation of NF-κB in the crypts. When tissue sections prepared from mouse distal colons of uninfected mice and of mice at days 3 and 7 after *C. rodentium* infection were stained with antibody for $p65^{276}$, we observed diffuse cytoplasmic and nuclear staining at day 3 but significant nuclear staining at day 7 (Fig. 2D), thereby coinciding with NF-κB activation kinetics. In addition to crypt immunoreactivity, however, we also observed significant staining of $p65^{276}$ in the subepithelial region, suggesting compartmentalization in the stroma. These immunohistochemical stainings were specific as control experiments with either rabbit IgG or involving omission of primary antibody did not exhibit any nonspecific staining (see Fig. S1 in the supplemental material). To implicate stroma in NF-κB activation, we next performed a study involving isolation of crypts and CLP from uninfected mice and from mice at various days after *C. rodentium* infection as described previously (11) and used them for histology or immunohistochemistry while cellular/nuclear extracts were prepared for biochemical assays. As shown in Fig. 3A (upper panel), H&E-stained sections from uninfected or *C. rodentium*-infected distal colons were completely devoid of crypts, reflecting the efficiency of the crypt isolation procedure. Interestingly, significant recruitment of polymorphonuclear neutrophils (PMNs) and other myeloid/immune cells was recorded in CLP at days 5 and 7 compared to levels in uninfected controls, suggesting inflammation-associated changes at these time points. When these sections were stained for Ki-67, significant increases in proliferation of various immune cells were recorded at days 5 and 7 compared to levels in uninfected controls (Fig. 3A, lower panel). This is the first demonstration of changes observed in the stroma of a bacterial infection-induced colitis model. Next, we determined NF-κB activity both in the crypts and in the CLP. As shown in Fig. 3B, a sequential increase in NF-κB activity starting at day 1 with continued increase until day 7 was observed in the CLP. Interestingly, when NF-κB activity was measured in the crypts, the early kinetics at days 1 and 3 were exact replicas of those recorded in the CLP (Fig. 3B). At day 5 and particularly at day 7, however, we observed significant enhancement of NF-κB activity in the crypts over that recorded in the CLP (Fig. 3B). Similar to findings in crypts, no appreciable change in IκBα phosphorylation or degradation was recorded in CLP (data not shown). To determine the phosphorylation status of the p65 subunit in the two preparations, both crypts and CLP cellular and nuclear extracts were blotted for Ser-276 and Ser-536 moieties, respectively. As expected, cellular

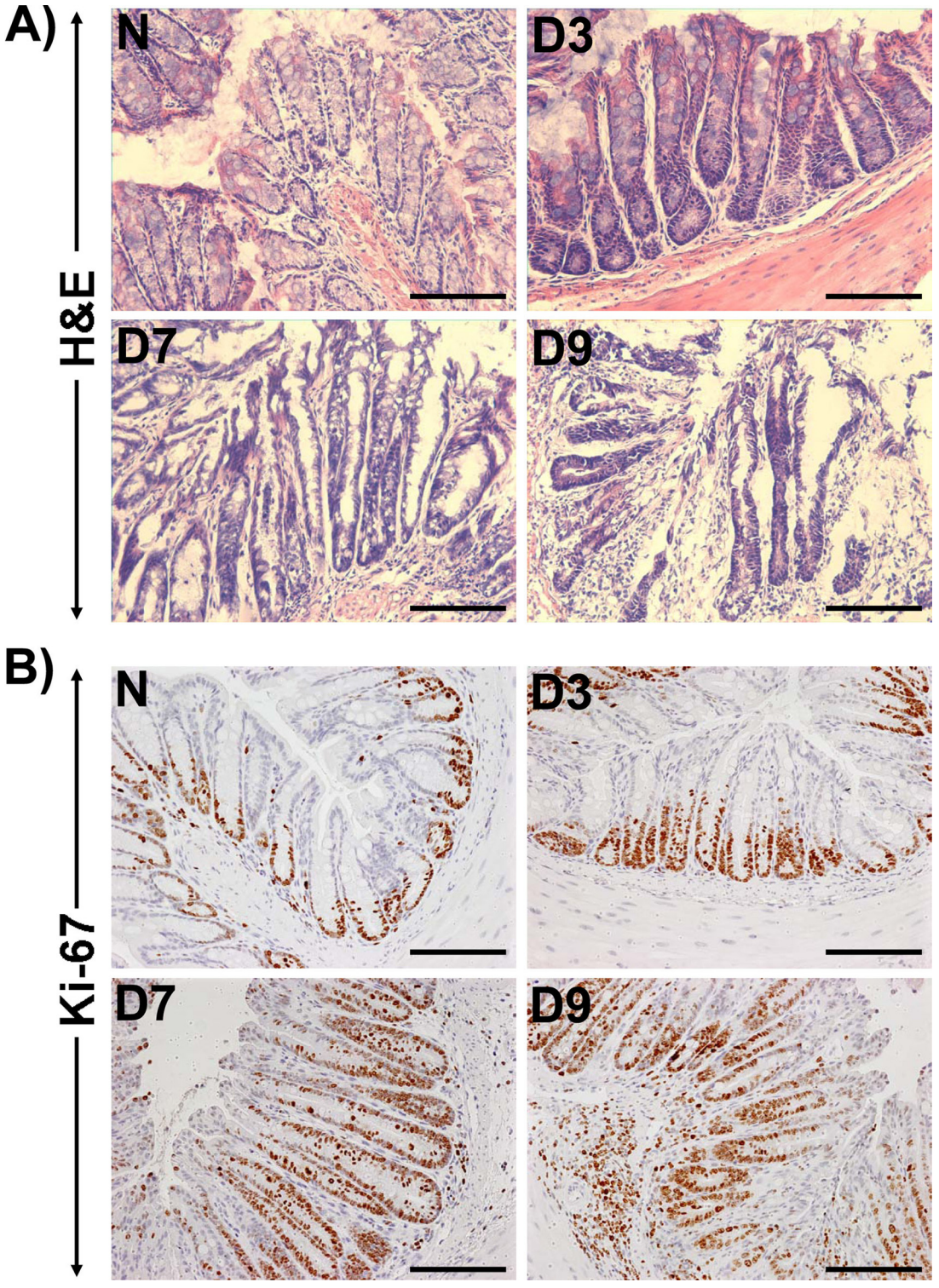

FIG 1 Hyperplasia precedes inflammation in an inbred mouse strain genetically susceptible to inflammation and/or colitis. (A) H&E staining in the paraffin-embedded sections prepared from the distal colons of uninfected healthy (N, for normal) and *C. rodentium* (CR)-infected (days 3 to 9 [D3 to D9]) C3H inbred mice. Scale bar, 75 μm. (B) Crypt hyperplasia as measured by immunohistochemical labeling of Ki-67 as a marker of proliferation in the paraffin-embedded sections prepared from the distal colons of uninfected and *C. rodentium*-infected (days 3 to 9) C3H mice. Scale bar, 75 μm ($n = 3$ independent experiments).

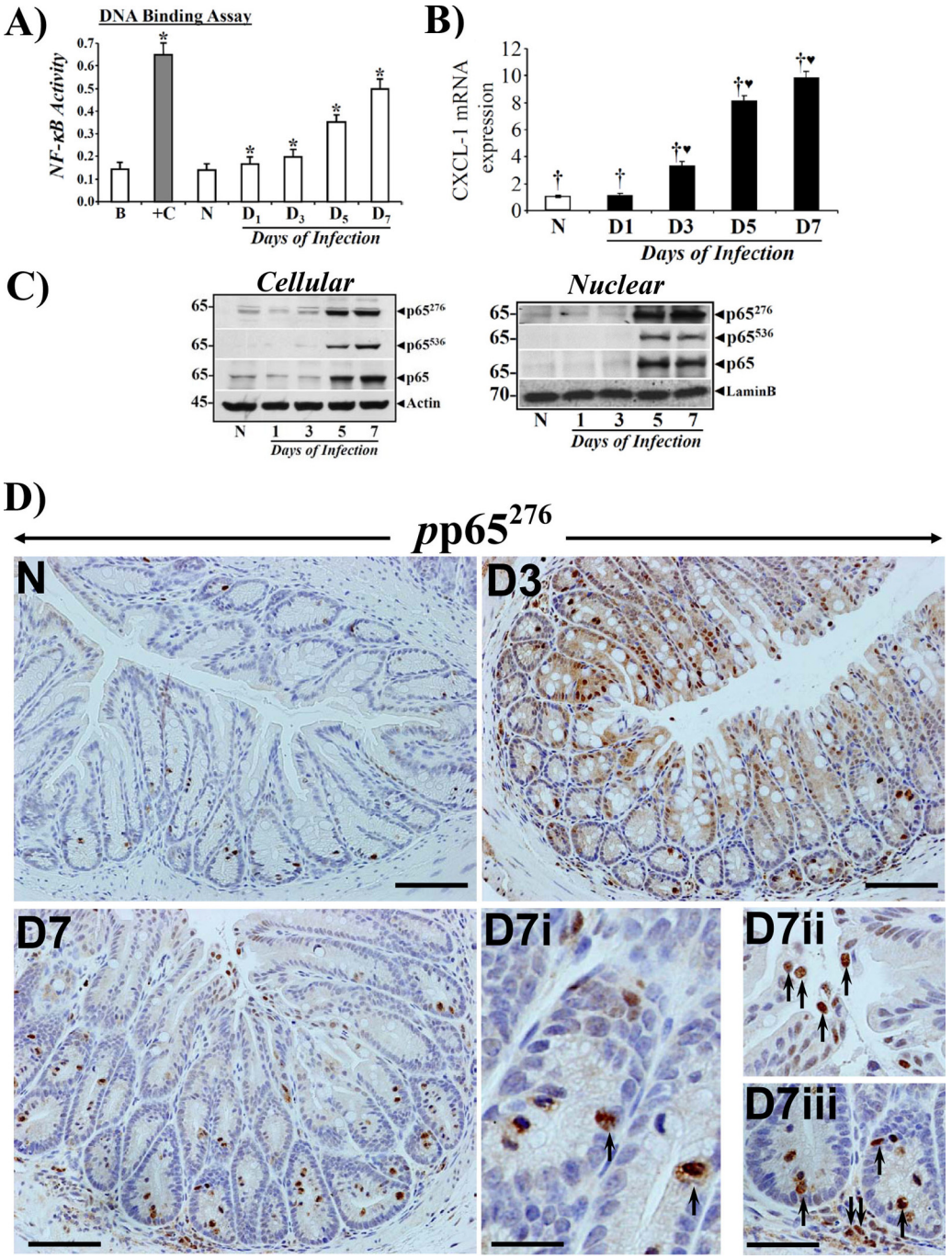

FIG 2 Crypt hyperplasia in C3H mice in response to *C. rodentium* infection correlates with increases in NF-κB activity and subunit expression. (A) Nuclear extracts were prepared from the isolated crypts of uninfected healthy (N) mice and of mice at days 1 to 7 postinfection and assayed for NF-κB activity via a TransAM NF-κB-p65 Chemi Transcriptional Factor assay kit from Active Motif ($n = 3$; *, $P < 0.05$ versus control). (B) Real-time RT-PCR. Expression of CXCL-1/KC mRNA isolated from the crypts of the animals described for panel A was measured as a readout for NF-κB activity via real-time RT-PCR. †♥, $P < 0.05$ versus control (†) ($n = 3$ independent experiments). (C) Phosphorylation status of the p65 subunit *in vivo*. Relative levels of cellular and nuclear p65 subunit phosphorylated at Ser-276 and -536 ($p65^{276}$/$p65^{536}$) along with the total p65 subunit were determined in the colonic crypt extracts prepared from uninfected healthy (N) mice and from mice at days 1 to 7 postinfection by Western blotting ($n = 3$ independent experiments). (D) Immunohistochemical staining of the p65 subunit phosphorylated at Ser-276 *in vivo*. Paraffin-embedded sections prepared from mouse distal colons of uninfected healthy (N) mice and of mice at days 3 to 7 postinfection were stained with antibody specific for NF-κB p65 phosphorylated at Ser-276 ($pp65^{276}$) and were analyzed with light microscopy. Magnifications, ×200 (D3 to D7) and ×400 (D7i to D7iii showing crypt and stromal staining). $n = 3$ independent experiments.

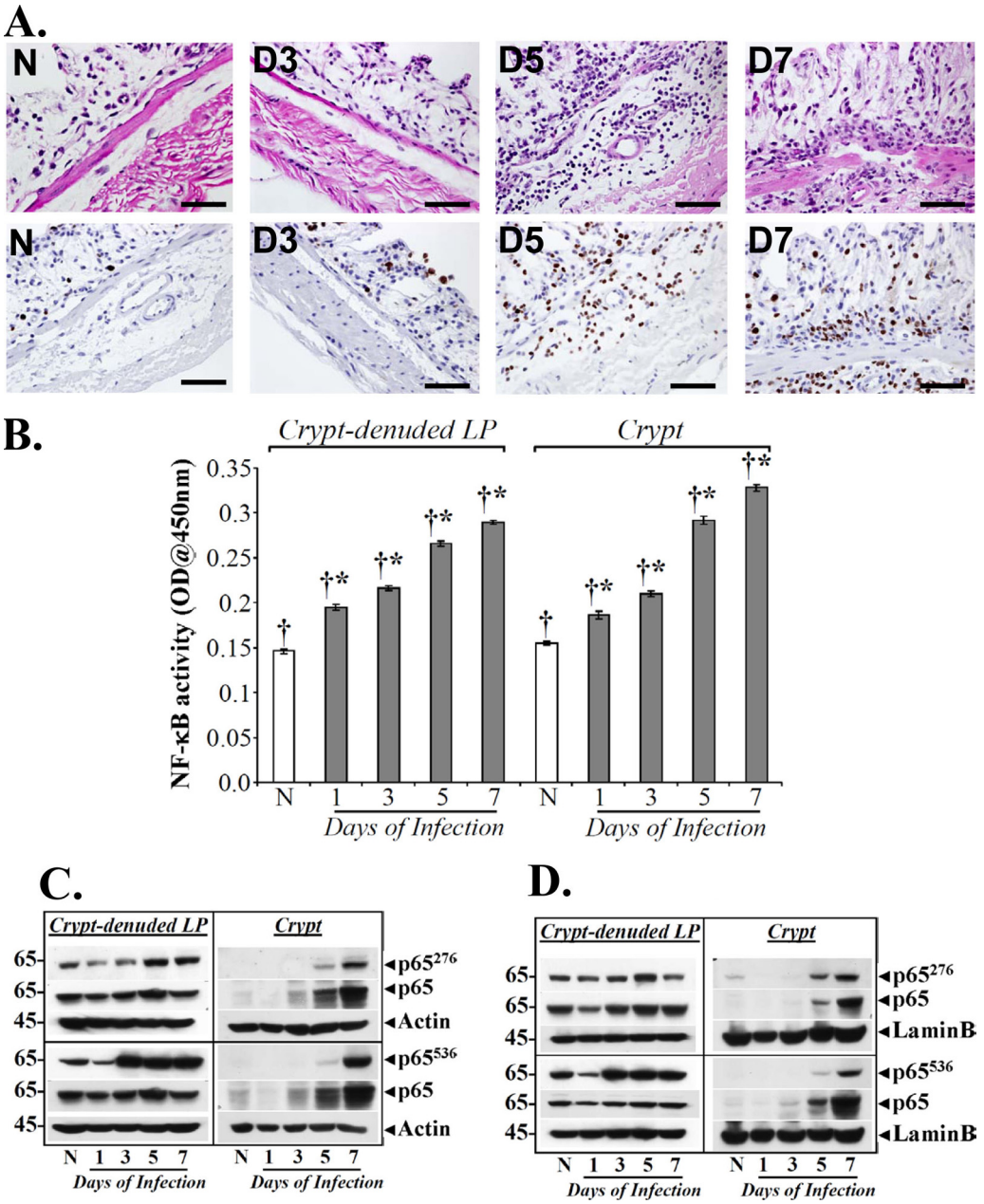

FIG 3 Separation of crypts and CLP from the distal colons of C3H mice. (A) H&E staining (upper panel) of the CLP prepared from the distal colons of uninfected healthy (N) and *C. rodentium*-infected (days 1 to 7) C3H mice. Scale bar, 100 μm; $n = 3$. The lower panel shows immunohistochemical labeling of Ki-67 as a marker of proliferation in the paraffin-embedded sections prepared from the distal colons of CLP of uninfected healthy (N) and *C. rodentium*-infected (days 1 to 7) C3H mice. Scale bar, 100 μm. (B) NF-κB activities measured in the CLP and crypts via a DNA binding assay. NF-κB p65 activities in the nuclear extracts of crypts and CLP from uninfected healthy (N) C3H mice and mice at days 1 to 7 postinfection were examined by utilizing a TransAM NF-κB p65 Chemi Transcriptional Factor assay kit from Active Motif. †*, $P < 0.05$ versus control (*); $n = 3$. OD, optical density (C and D) Kinetics of p65 phosphorylation at Ser-276 and -536 in the two compartments *in vivo*. Relative levels of phosphorylated ($p65^{276}$/$p65^{536}$) and total p65 subunit in the cellular (C) and nuclear (D) extracts prepared from isolated crypts and CLP of uninfected healthy (N) C3H mice and mice at days 1 to 7 postinfection were determined by Western blotting.

and nuclear $p65^{276}$, despite exhibiting a lack of significant change in abundance in CLP, was at least detectable in both cellular and nuclear fractions at days 1 and 3, in contrast to the inability to detect this moiety in the crypts (Fig. 3C and D). This is consistent with crypt data reported in Fig. 2. At day 5 however, $p65^{276}$ increased significantly in the CLP in both fractions (Fig. 3C and D). Interestingly, nuclear levels of $p65^{276}$ declined at day 7 in the CLP, unlike levels recorded in the crypts (Fig. 3C and D). When the status of $p65^{536}$ was examined in the CLP and crypts, we observed dramatic increases in $p65^{536}$ levels in the CLP at day 3 in both cellular and nuclear fractions, with sustained levels at days 5 and 7 of TMCH (Fig. 3C and D). In the crypts, on the other hand, $p65^{536}$ was undetectable at days 1 and 3 and barely detectable at day 5 in either the cellular or nuclear fraction (Fig. 3C and D). At day 7,

however, a significant increase in $p65^{536}$ was observed in both crypt cellular and nuclear fractions, and, similar to $p65^{276}$, $p65^{536}$ also exhibited sustained increases at this time point (Fig. 3C and D). Unlike levels in the crypts, however, Ser-536 exhibited significantly more phosphorylation than Ser-276, suggesting that $p65^{536}$ may be more relevant in regulating NF-κB activity in the CLP. These studies further implicate stromal-epithelial components in the regulation of NF-κB activity following *C. rodentium* infection.

To clearly understand the cell types in CLP with the activated form of p65, we next stained CLP sections with antibody for $p65^{276}$. As shown in Fig. S2 in the supplemental material, CLP from uninfected animals did not exhibit any significant staining for $p65^{276}$. Between days 1 and 5, we observed dramatic increases in $p65^{276}$ staining, mostly in regions denuded for crypts (see Fig. S2). At day 7, however, staining was mostly restricted to the basal lamina and submucosal regions (see Fig. S2). The majority of the staining for $p65^{276}$ at days 5 and 7 was observed either in lymphocytes or macrophages while infiltrating granulocytes (mostly neutrophils), metamyelocytes, and rare eosinophils also stained positive for $p65^{276}$ (see Fig. S3). The presence of lymphocytes and macrophages was further confirmed by staining of CLP sections with antibodies for CD3 and F4/80, respectively (see Fig. S4A and B). As readout for changes in NF-κB activity, we next examined the cytokine/chemokine profile in the colonic extracts to further dissect the contribution of the epithelium and the stroma in regulating hyperplasia and/or colitis during TMCH. Our results revealed that interleukin-12p40 (IL-12p40), a subunit of IL-12 family of cytokines which are upregulated in the Th1-mediated models of IBD (24), exhibited cyclical expression, with expression increasing initially at day 1 and particularly at day 3 before declining at day 5 (Fig. 4A); at days 7 and 9, however, we again observed a gradual increase in its expression (Fig. 4A). IL-12p40 is predominantly expressed by macrophages and dendritic cells (DCs) in addition to monocytes, neutrophils, and keratinocytes, suggesting that the lamina propria representing the stroma may have been activated following *C. rodentium* infection. Other cytokines or chemokines with significant increases recorded during TMCH were IL-1α/β, IL-6, IL-9, granulocyte colony-stimulating factor (G-CSF), macrophage inflammatory protein 1α (MIP-1α), monocyte chemotactic protein 1 (MCP-1), and KC, which may be a result of NF-κB activation in response to *C. rodentium* infection. Since intestinal dendritic cells sample bacteria and are recruited within the lamina propria following pathogenic insult, we performed an NF-κB reporter assay using a dendritic cell line (JAWSII) to determine if NF-κB is indeed activated in response to *C. rodentium* infection in parallel with YAMC cells, a simian virus 40 (SV40)-immortalized epithelial cell line for comparison. YAMC and JAWSII cells exhibited 3.5- and 2.2-fold increases in reporter activity, respectively, following *C. rodentium* infection compared to levels in uninfected controls (Fig. 4B). Next, we performed a coculture study to definitively implicate stromal-epithelial interactions in the regulation of NF-κB activity in response to *C. rodentium* infection. As shown in Fig. 4Ci, while YAMC cells were epithelial, CLP cells exhibited a fibroblast-like appearance, as determined by staining for α-smooth muscle actin (α-SMA) and vimentin (data not shown). When YAMC and CLP cells were cocultured in the absence of *C. rodentium* infection, we did not observe any increase in NF-κB activity over that recorded in YAMC or CLP cells alone (Fig. 4Cii). In response to *C. rodentium* infection, we observed a 2-fold increase in NF-κB activity in coculture of YAMC and CLP (YAMC+CLP) cells compared to YAMC+CLP alone (Fig. 4Cii). This increase in NF-κB activity in the *C. rodentium*-infected YAMC+CLP group was still higher than that recorded in either the *C. rodentium*-infected YAMC or *C. rodentium*-infected CLP. Thus, both crypt and the CLP apparently act in tandem to regulate NF-κB activation following *C. rodentium* infection. Since upregulation of chemokines such as MCP-1 and CXCL-1/KC is primarily associated with recruitment of neutrophils and other leukocytes to the colonic mucosa, we next measured MPO activity as the global marker of leukocyte accumulation. Compared to the uninfected control, a sequential increase in MPO activity was recorded (Fig. 4D) at time points which coincided with increases in KC and MCP-1 levels (Fig. 4A), suggesting that MCP-1 and KC may be the major players in regulating leukocyte recruitment and propagation of inflammation in C3H mice in response to *C. rodentium* infection.

We have recently shown that the MEK/ERK/p38 pathway is involved in NF-κB activation during progression and regression phases of hyperplasia in NIH/Swiss outbred mice (11). MAPK cascades cooperate in the orchestration of inflammatory responses during IBD (37) and p38-MAPK has recently been shown to contribute toward the immune responses against enteric infection (16). We therefore examined changes in these kinases in both crypts and CLP to further study how *C. rodentium* infection affects signaling via these kinases in the two compartments. As shown in Fig. 5, we did not observe any measurable increase in either cellular or nuclear phospho-p38 (pp38) or phospho-p44/42 (pp44/42) at days 1 and 3 in the crypts. At days 5 and 7, however, dramatic increases in both cellular and nuclear pp38 and pp44/42 were observed in the crypts (Fig. 5A), which correlated with increases in both $p65^{276}$ and $p65^{536}$ as well as with NF-κB activity at these time points. These findings were confirmed by immunohistochemical staining of paraffin-embedded sections, where diffuse crypt labeling mostly restricted to the crypt surface in either uninfected crypts or at day 1 was followed by more nuclear staining extending along the length of the colonic crypts at days 5 and 7 (Fig. 5B). In the CLP, in contrast, early kinetics for activation of these kinases at days 1, 3, and 5 were observed in both cellular and nuclear fractions, followed by a significant decline to baseline at day 7 (Fig. 5C). These biochemical findings were confirmed by immunohistochemical staining of the CLP with antibodies specific for pp38 and pp44/42, as shown in Fig. 5D. To further assess the role of p44/42-MAPK and p38 MAPK in the regulation of NF-κB activity in the two compartments, both uninfected (data not shown) and *C. rodentium*-infected C3H mice were treated with inhibitors specific for ERK-1/2 (PD98059 [PD]) and p38 (SB203580 [SB]) for 5 days starting at 2 days post-*C. rodentium* infection, as described in Materials and Methods. Both PD and SB significantly blocked increases in relative levels of p44/42 and p38 MAPKs in the crypts (Fig. 6A). In the CLP, however, while p38 inhibition was more effective than p44/42 (Fig. 6A), the inhibitory effect of SB was less prominent in the CLP than in the crypts. Next, a series of experiments investigated the effect of MAPK inhibitors on cell proliferation, NF-κB activity, and CXCL-1 mRNA expression in the two compartments. Both PD and SB significantly reduced crypt cell proliferation, as revealed by Ki-67 staining, compared to *C. rodentium* infection alone (Fig. 6B). This could be due to decreases in NF-κB activity as both PD and SB significantly inhibited NF-κB activity in the two compartments (Fig. 6C and D). Interestingly,

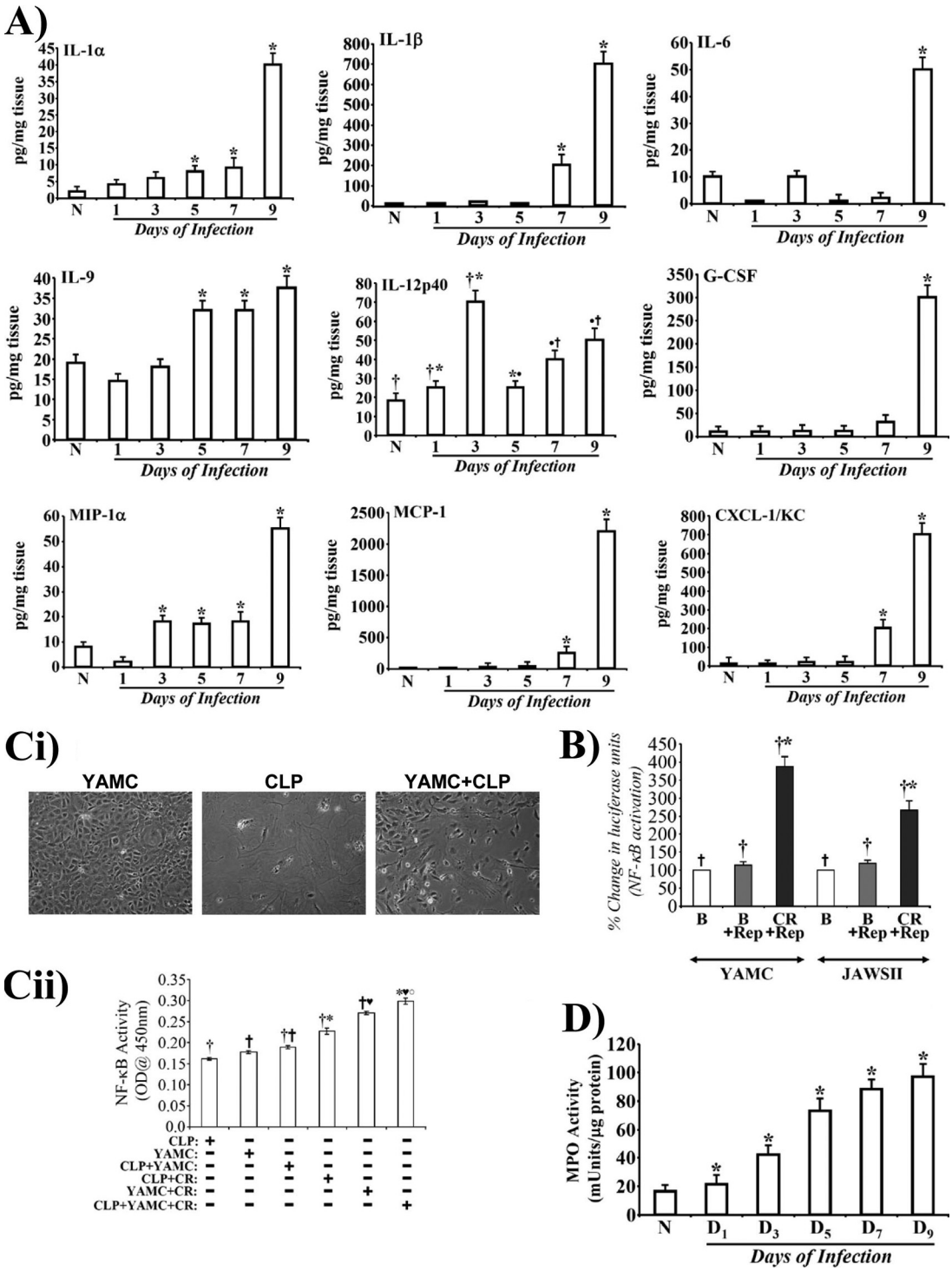

FIG 4 Distinct cytokine/chemokine expression and stromal-epithelial interaction in the regulation of NF-κB activity *in vivo*. (A) Expression of proinflammatory cytokines and chemokines in the distal colonic homogenates of uninfected healthy (N) and *C. rodentium*-infected (days 1 to 9) mice were measured using a Bio-Plex Cytokine assay kit as described by the manufacturer. Samples were analyzed on a Bio-Rad 96-well plate reader using a Bio-Plex array system and Bio-Plex Manager software. Each bar represents mean ± standard deviation. *, $P < 0.05$ versus control; †*, $P < 0.05$ versus the control (†) ($n = 3$). (B) Luciferase reporter assay to measure relative activation of NF-κB in response to *C. rodentium* infection. Both YAMC and JAWSII cell lines were transfected with pGL4.32(luc2P/NF-κB-RE/Hygro) vector for 36 h. The transfected cells were treated with or without *C. rodentium* for 3 h, washed to remove bacteria, and processed for measuring the relative levels of luciferase. The NF-κB activity changes are presented as percent change in luciferase units ($n = 3$ independent experiments). (C) Growth of YAMC and CLP cells *in vitro* (i) Both YAMC and CLP cells were propagated in appropriate medium at 33 and 37°C, respectively. For coculture studies, YAMC cells were layered onto CLP at a ratio of 1:1, and cocultures were incubated at 37°C for 24 h. Untreated or *C. rodentium*-infected cells were used to measure NF-κB activity via a TransAM NF-κB-p65 Chemi Transcriptional Factor assay from Active Motif (ii). †*, $P < 0.05$ versus control (†); †♥, $P < 0.05$ versus control (†), *♥○, $P < 0.05$ versus *C. rodentium*-infected CLP (CLP+CR) or *C. rodentium*-infected YAMC (YAMC+CR) (†* or †♥, respectively) ($n = 3$ independent experiments). (D) Measurement of MPO as a readout for assaying the extent of neutrophil recruitment to the colonic mucosa. MPO activity was measured in the colonic homogenates of uninfected healthy (N) and *C. rodentium*-infected (days 1 to 9) mice using a Fluoro MPO detection kit (Cell Technology, Inc., CA) according to the manufacturer's protocol. Each bar represents mean ± standard deviation (*, $P < 0.05$; $n = 3$ independent experiments).

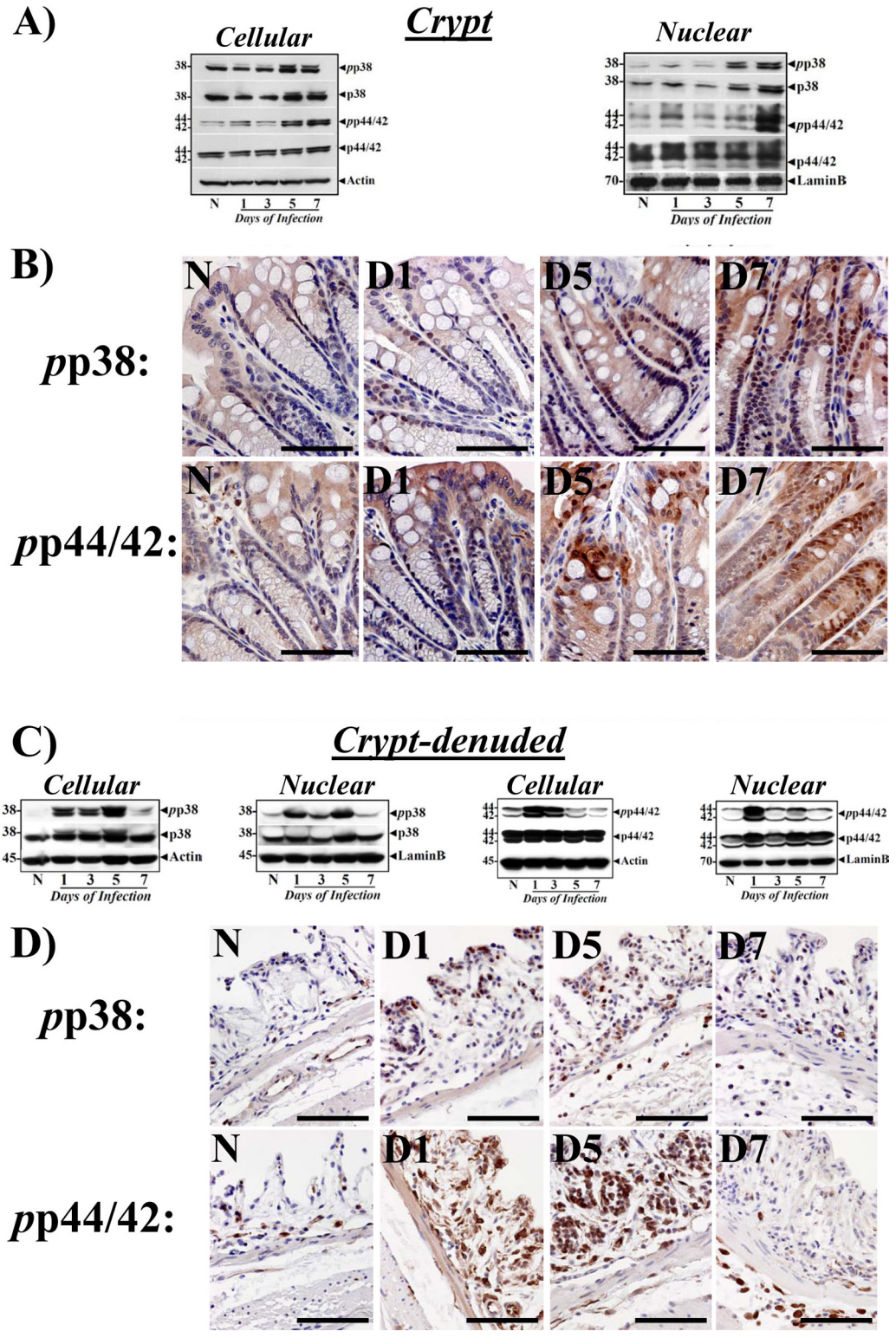

FIG 5 Biochemical and immunohistochemical measurement of changes in the relative levels of p38-MAPK and p44/42-ERK during TMCH. Cellular and nuclear extracts (A and C) prepared from the crypts and CLP from the distal colons of uninfected healthy (N) mice of mice at days 1 to 7 postinfection were analyzed for the relative abundance of p38 and p44/42-ERK proteins by Western blot analysis ($n = 3$ independent experiments). (B and D) Immunohistochemical staining for pp38 and pp44/42 in the paraffin-embedded sections prepared from either whole distal colons (B) or CLP (D) of uninfected healthy (N) and *C. rodentium*-infected (days 1 to 7) C3H mice. Scale bar, 25 μm; $n = 3$ independent experiments.

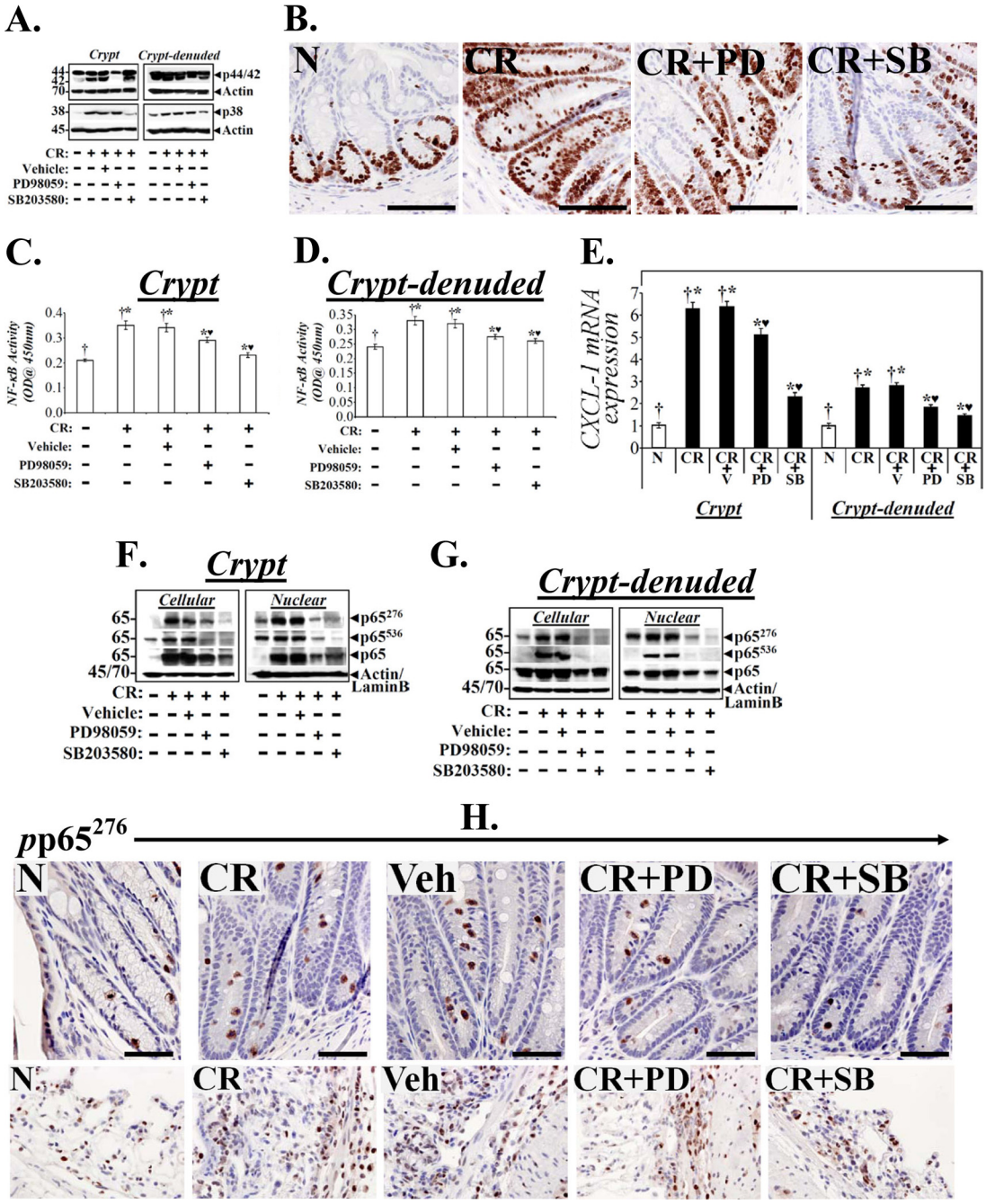

FIG 6 Effect of p44/42-ERK1/2 and p38 inhibition on cell proliferation and NF-κB activity *in vivo*. Uninfected or *C. rodentium*-infected-infected C3H mice were injected once a day for 10 days with either vehicle or inhibitors specific for ERK1/2 (PD) or p38 (SB). At 2 h after the last injection, colonic crypts and CLP were isolated. (A) Representative Western blots showing total ERK1/2 and p38 in the two compartments. (B) Representative photomicrographs of paraffin-embedded sections stained with antibody to Ki-67: N, uninfected healthy mice; CR, *C. rodentium*-infected mice; CR+PD or CR+SB, *C. rodentium*-infected mice treated with specific ERK1/2 or p38 inhibitor. Scale bar = 50 μm (n = 3 independent experiments). (C and D) NF-κB activities measured via DNA binding assay in the crypts and CLP. Each bar represents mean ± standard deviation. †*, $P < 0.05$ versus control (†); *♥, $P < 0.05$ versus CR (†*) (n = 3). (E) Real-time RT-PCR. CXCL-1 expression in the crypts and CLP were measured via real-time RT-PCR. †*, $P < 0.05$ versus control (†); *♥, $P < 0.05$ versus *C. rodentium*-infected, vehicle-treated mice (CR+V; †*) (n = 3 independent experiments). (F and G) Crypts and CLP cellular and nuclear extracts prepared from the distal colons of the above group of animals were analyzed by Western blotting with antibodies specific for total p65 or the p65 subunit phosphorylated at Ser 276 ($p65^{276}$) or Ser 536 ($p65^{536}$). Actin or lamin B was the loading control, respectively (n = 3 independent experiments). (H) Representative photomicrographs of paraffin-embedded sections stained with antibody specific for phosphorylated $p65^{276}$ ($pp65^{276}$): N, uninfected healthy; CR, *C. rodentium*-infected; Veh, *C. rodentium*-infected and vehicle-treated; CR+PD or CR+SB, *C. rodentium*-infected and treated with specific ERK1/2 or p38 inhibitor, respectively. Scale bar = 30 μm (n = 3 independent experiments).

p38 inhibition was more effective than p44/42 in either reducing proliferation or NF-κB activity in either compartment (Fig. 6B to D). The blocking of NF-κB activities by the two inhibitors also affected expression of its downstream target as SB blocked CXCL-1 mRNA expression almost completely in the crypts and to a significant extent in the CLP (Fig. 6E) while PD was equally effective in both the compartments (Fig. 6E). To examine how these interventions affected the NF-κB p65 subunit, we next probed the crypts and CLP cellular and nuclear fractions with antibodies to total protein and the p65 subunit phosphorylated at Ser-276 and -536. Both the total protein and phosphorylated p65 subunit were blocked by PD and SB in the crypts and CLP. Moreover, SB was more effective than PD in blocking increases in either $p65^{276}$ or $p65^{536}$, and inhibition of $p65^{536}$, particularly in the CLP, was more profound than that of $p65^{276}$ (Fig. 6F and G). These results suggest that while both phosphorylated moieties may have contributed toward functional NF-κB activation in the two compartments, $p65^{276}$ may be more relevant in regulating NF-κB activity in the crypts while $p65^{536}$ may be more important in the CLP. These results were also confirmed by immunochemical staining of the $p65^{276}$ subunit in the two compartments. As shown in Fig. 6H, significant staining for $p65^{276}$ was recorded in both *C. rodentium*-infected and *C. rodentium*-infected, vehicle-treated sections compared to staining in uninfected controls. Both PD and SB significantly blocked increases in $p65^{276}$ in the crypts even though SB was relatively more effective than PD (Fig. 6H). In the CLP, however, PD was more effective than SB, despite some residual staining observed for $p65^{276}$ in both PD- and SB-treated CLP (Fig. 6H). To clearly understand if inhibition of NF-κB activities in the two compartments affected the recruitment of infiltrating cells in the mucosa, we next stained sections from the same group of animals with antibodies for CD3 and F4/80 to detect T cells and macrophages, respectively. Both PD and SB significantly blocked increases in either $CD3^+$ T cells or F4/80-positive ($F4/80^+$) macrophages either in the stroma or along the length of the colonic crypts (see Fig. S5 in the supplemental material), suggesting that early targeting of the NF-κB-dependent processes can help ameliorate inflammatory cascades.

We have shown previously that diet containing 6% soluble fiber pectin completely blocked increases in β-catenin levels and NF-κB activity, thereby abrogating *C. rodentium*-induced hyperplasia in NIH/Swiss outbred mice (29, 11). In the current study, we hypothesized that both pectin and curcumin, the principal curcuminoid of the popular Indian spice turmeric, will ameliorate inflammation and minimize morbidity and mortality in genetically susceptible C3H mice in response to *C. rodentium* infection. As is shown in Fig. S6A and B in the supplemental material, *C. rodentium* infection of C3H mice for 9 days induced significant expansion of $CD3^+$ T cells and recruitment of $F4/80^+$ macrophages in the stroma compared to levels in uninfected controls. Both a 6% pectin and 4% curcumin diet significantly blocked increases in these molecules (see Fig. S6A and B). At the same time, mucosal inflammation and infiltration of polymorphonuclear cells in the *C. rodentium*-infected group was significantly attenuated by both pectin and curcumin, as revealed by measuring the histology scores following hematoxylin and eosin (H&E) staining of colonic sections (Fig. 7A; see also Fig. S6C). Interestingly, we observed significant crypt hyperplasia in both pectin- and curcumin-treated animals, suggesting that these dietary interventions, while being anti-inflammatory, may be promoting crypt recovery following the colitic insult. To confirm that these diets were indeed promoting proliferation, colonic sections were stained with antibody for Ki-67. As shown in Fig. 7B, we observed dramatic increases in Ki-67 staining in sections prepared from both pectin- and curcumin-treated animals compared to staining in untreated mice, thereby correlating with increases in crypt lengths. At the same time, when a terminal deoxynucleotidyltransferase-mediated dUTP-biotin nick end labeling (TUNEL) assay to measure apoptosis was performed, there was a significant reduction in the number of cells undergoing inflammation-induced apoptosis in sections from treated versus untreated animals (Fig. 7C). To understand the mechanistic basis of increases in crypt hyperplasia in response to dietary intervention, we next investigated changes in NF-κB activity in the crypts from various groups. As shown in Fig. 7D, NF-κB activity, measured via a DNA binding assay, increased reproducibly in colonic crypts from *C. rodentium*-infected mice compared to activity in uninfected controls. Interestingly, NF-κB activity was either equal to (with 6% pectin) or even greater (with 6% curcumin) than that recorded with infection alone (Fig. 7D). To correlate changes in NF-κB activity with presence/absence of phosphorylated p65 NF-κB subunit in the nucleus, we next stained colonic sections from various groups with antibody to $p65^{276}$. As shown in Fig. 7E, $p65^{276}$ nuclear staining increased significantly at day 9 compared to uninfected control while neither pectin nor curcumin abrogated nuclear localization of $p65^{276}$, which correlated with the lack of inhibitory effect of these diets on NF-κB activity in the crypts (Fig. 7D). When the effect of dietary intervention on cytokine/chemokine expression in the colon of C3H mice was investigated, both the pectin and curcumin diets significantly blocked increases in IL-1α/β, G-CSF, MCP-1, and CXCL-1/KC (see Fig. S7A in the supplemental material), leading to significant decreases in MPO activity in treated versus untreated mice (see Fig. S7B). We have further observed that none of these diets had any inhibitory effect on either bacterial binding or infectivity (see Fig. S8).

DISCUSSION

Bacterial pathogens are endowed with the ability to colonize host cells, ultimately leading to cellular damage (14). Following penetration into a susceptible host, pathogens must elude host immunological responses, on one hand, and successfully compete with the commensal population, on the other. Thus, multiplication of bacterial pathogens in the host may depend on survival strategies which will determine the success of the infectious process. Infection of laboratory mice with *C. rodentium* provides a useful *in vivo* strategy to investigate the pathogenesis of human idiopathic inflammatory bowel disease (IBD) and for preclinical evaluation of candidate preventive and therapeutic agents (7).

The biological functions of colonic crypt cells under intestinal inflammatory conditions vary significantly depending upon several factors, such as the phase of colitis (acute versus recovery versus chronic) and the fundamental mechanism of colitis development (Th1 versus Th2 contributions) (20). The proliferation of these cells is controlled by several signaling molecules. NF-κB signaling has been implicated in the pathogenesis of acquired immune-mediated colitis (22) and dextran sodium sulfate (DSS)-induced intestinal injury (27). Given the double-edged functioning of various signaling cascades in colitis, it is imperative that we clearly understand the cell population that is being targeted when we consider the activation or inhibition of NF-κB in response to

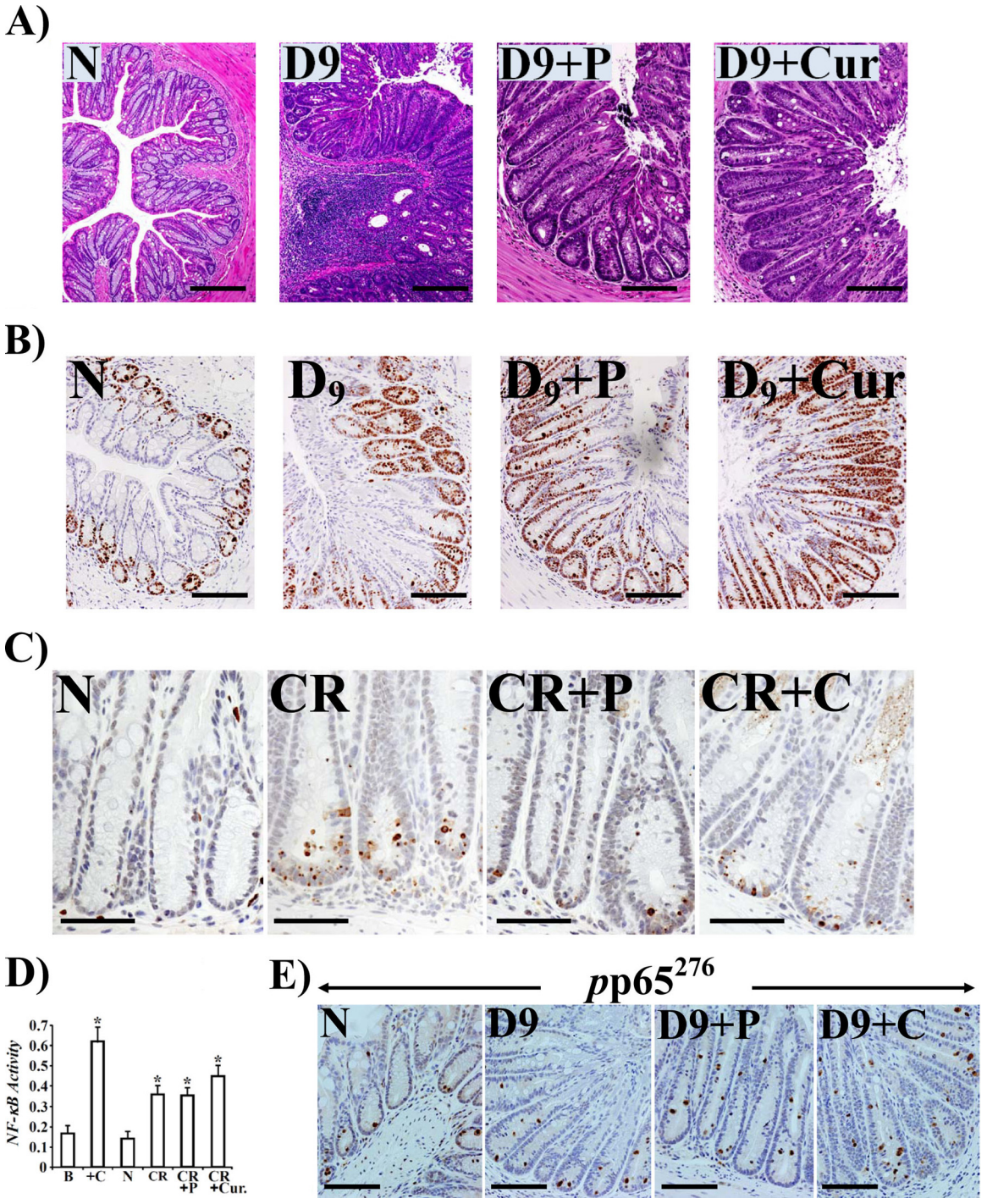

FIG 7 Anti-inflammatory and proproliferatory properties of pectin and curcumin diets. Paraffin-embedded sections prepared from the distal colons of uninfected healthy (N) mice, *C. rodentium*-infected mice at day 9 postinfection (D9), and *C. rodentium*-infected mice at day 9 treated with 6% pectin or 4% curcumin diets (D9+P or D9+Cur, respectively) were stained with H&E (A), stained for Ki-67 (B), or examined for apoptosis via TUNEL assay (C). Scale bar, 50 μm; $n = 3$. In panel B, please note significant increases in Ki-67 staining demonstrating proproliferatory activities of both pectin and curcumin. In panel C, please note significant inhibition of apoptosis in treated samples. (D) Both the pectin and curcumin diets promote NF-κB activity in the crypts. Colonic crypt NF-κB p65 activity in the nuclear extracts prepared from uninfected healthy (N) mice, *C. rodentium*-infected mice, and *C. rodentium*-infected mice treated with 6% pectin (P) or 4% curcumin (Cur) was measured by utilizing a TransAM NF-κB p65 Chemi Transcriptional Factor assay kit from Active Motif. *, $P < 0.05$ versus control ($n = 3$). (E) Staining for p65 phosphorylated at Ser-276 ($pp65^{276}$) in the diet-treated samples. Panels show immunohistochemical staining of p65 phosphorylated at Ser-276 ($pp65^{276}$) in the paraffin-embedded sections prepared from the distal colons of uninfected healthy (N) mice, *C. rodentium*-infected mice at day 9, or *C. rodentium*-infected mice treated with a 6% pectin (D9+P) or 4% curcumin (D9+C) diet, respectively (scale bar, 75 μm; $n = 3$).

bacterial infection. Utilizing the *C. rodentium*-induced TMCH in NIH/Swiss mice, we recently characterized NF-κB activation during progression and regression phases of colonic crypt hyperplasia (11). In the current study, we have investigated in detail distinct compartmentalization of NF-κB activity in the crypts and CLP of C3H mice that exhibit extreme sensitivity to *C. rodentium* infection. The rationale for using C3H mice as opposed to either BALB/c or C57BL/6 mice was twofold: (i) C3H mice develop an overly aggressive response to *C. rodentium* infection and therefore exhibit an IBD-like phenotype; (ii) we wanted to determine if these mice, despite being genetically more susceptible, would respond to chemical or dietary interventions. Following *C. rodentium* infection, we observed a biphasic response of hyperplasia preceding inflammation. Measurement of NF-κB activation kinetics also revealed an early and a relatively delayed response in the CLP and crypts, respectively. Specifically, NF-κB activity in the CLP (mostly in lymphocytes and infiltrating granulocytes) increased as early as day 1 postinfection, consistent with NF-κB being a latent transcription factor, while its activation in the crypts did not increase to any significant level until day 3 before peaking by day 7. During measurement of cytokines/chemokines in the inflamed colon, increases in IL-1α, IL-12(p40), and MIP-1α paralleled NF-κB activation while increases in IL-1α/β, IL-6, IL-12(p40), G-CSF, KC, MCP-1, and MIP-1α followed NF-κB activation. Since the majority of these proinflammatory cytokines or chemokines are expressed by cells of the lamina propria and the epithelium, NF-κB activation at these sites following *C. rodentium* infection may reflect the bidirectional signaling across the basement membrane, which may be integral to regulating hyperplasia and/or colitis in these mice. Indeed, the coculture studies involving both YAMC epithelial and CLP stromal cells revealed a significant additive effect on NF-κB activity. In a recent study, Boquoi et al. (6), using transgenic mice overexpressing vascular endothelial growth factor (VEGF) in the epithelial cells, showed that epithelial-mesenchymal cross talk regulates proliferation of normal and neoplastic epithelium. Similarly, Maaser et al. (18) showed in an *in vitro* coculture system that the epithelial-endothelial cell cross talk regulates expression of various adhesion molecules in an NF-κB-dependent manner. Since stromal/epithelial cross talk is required and is fundamental to regulating gut homoeostasis, our results corroborate well with previous studies and provide direct evidence of stromal-epithelial interaction in the regulation of NF-κB activity following a pathogenic insult.

We have recently shown that NF-κB activation in the colonic crypts of NIH/Swiss mice involved both canonical (during progression) and atypical (during regression) pathways (11). Since it is well documented that NF-κB can be activated in the absence of IκBα, IκBβ, or IκBε degradation (5, 13), we focused mainly on how phosphorylation of the NF-κB p65 subunit at Ser-276 and Ser-536 instead contributed toward functional NF-κB activation in the two compartments. Results of our study clearly show that phosphorylation of p65, particularly at Ser-276, was observed in not only the crypts but also the CLP. Interestingly, most of the staining for $p65^{276}$ in CLP was detected either in $CD3^+$ T-lymphocytes or $F4/80^+$ macrophages, which would have set the stage for distinct compartmentalization of NF-κB activity in the stroma (early increases in $p65^{276}$/$p65^{536}$ in the CLP) followed by NF-κB activation in the epithelium (delayed increase in $p65^{276}$/$p65^{536}$ in the crypts). Another interesting discovery was the extent to which p65 was phosphorylated at serine-276 or -536 in the two compartments. We found that p65 phosphorylation at Ser-276 was higher in the crypts, while a higher level of phosphorylation for Ser-536 than total p65 was recorded in the CLP. These findings indicate that $p65^{536}$ and not necessarily $p65^{276}$ may be regulating functional NF-κB activation in the CLP but that both moieties may be working in tandem to fully activate NF-κB in the CLP.

Major biological responses to inflammatory stimuli are integrated and conveyed by specific intracellular signals. Luminal bacteria and/or bacterial products enter the gastrointestinal wall and activate resident macrophages and epithelial cells of the crypts, inducing phosphorylation of MAPK (ERK1/2, Jun N-terminal protein kinase [JNK], and p38), thereby activating intracellular transcription factors such as NF-κB, STAT-3, and Egr-1, etc. (1). To further substantiate if signaling cascades involving ERK1/2 and p38 in addition to NF-κB are also compartmentalized in the crypt and crypt-denuded lamina propria following *C. rodentium* infection and to directly link changes in these MAPKs to NF-κB activity, we again utilized our expertise to systematically separate the two compartments for biochemical and immunohistochemical assays. It was interesting that the kinetics related to cellular and nuclear accumulation of phosphorylated ERK-1/2 and p38 coincided with those of $p65^{276}$ and $p65^{536}$ and suggested that these proteins may be the prime suspect in priming the inflammatory cascades in the mucosa by regulating NF-κB activation in the two compartments. Indeed, *in vivo* inhibition of both ERK1/2 and p38 with specific inhibitors not only interfered with p65 phosphorylation and NF-κB activity in the two compartments leading to abrogation of crypt hyperplasia but also reduced inflammation by preventing recruitment of immune and inflammatory cells to the mucosa. It has been shown recently by Docena et al. (12) that inflamed mucosa of IBD patients was associated with higher levels of phospho-p38α than those found in controls, and both mucosal biopsy specimens and LPMCs when incubated with selective p38α inhibitors exhibited significant blockade of p38α phosphorylation and expression of tumor necrosis factor alpha (TNF-α), IL-1β, and IL-6. Similarly, p38α has recently been shown to be a critical regulator of immune cell recruitment in the colonic mucosa (16). However, a systematic approach to link changes in intracellular signaling to the regulation of NF-κB activity *in vivo* in the mucosa following bacterial infection is lacking. Results of our study not only reiterate the significance of separating the lamina propria from the crypts in order to clearly understand how various cell types respond to a particular intervention but also suggest that the stroma, unless targeted early, presents a formidable challenge to a successful therapeutic intervention.

C. rodentium-induced TMCH, in addition to being an excellent *in vivo* model to study host-pathogen interactions under physiological conditions, also provides an opportunity to evaluate therapeutic interventions. Prior studies in our lab have shown that the TMCH model is diet sensitive and that dietary pectin (6%) blocks both β-catenin and NF-κB in the colonic crypts, thereby abrogating hyperplasia in NIH/Swiss mice (11, 29). However, it is not known if dietary intervention will be equally effective in ameliorating inflammation and/or colitis in genetically susceptible inbred strains. The aim of the present study was to examine the efficacy of 6% pectin and 4% curcumin diets in ameliorating the intestinal disease associated with *C. rodentium* infection *in vivo* and to determine whether their ameliorating effects are due in part to their action on NF-κB activity.

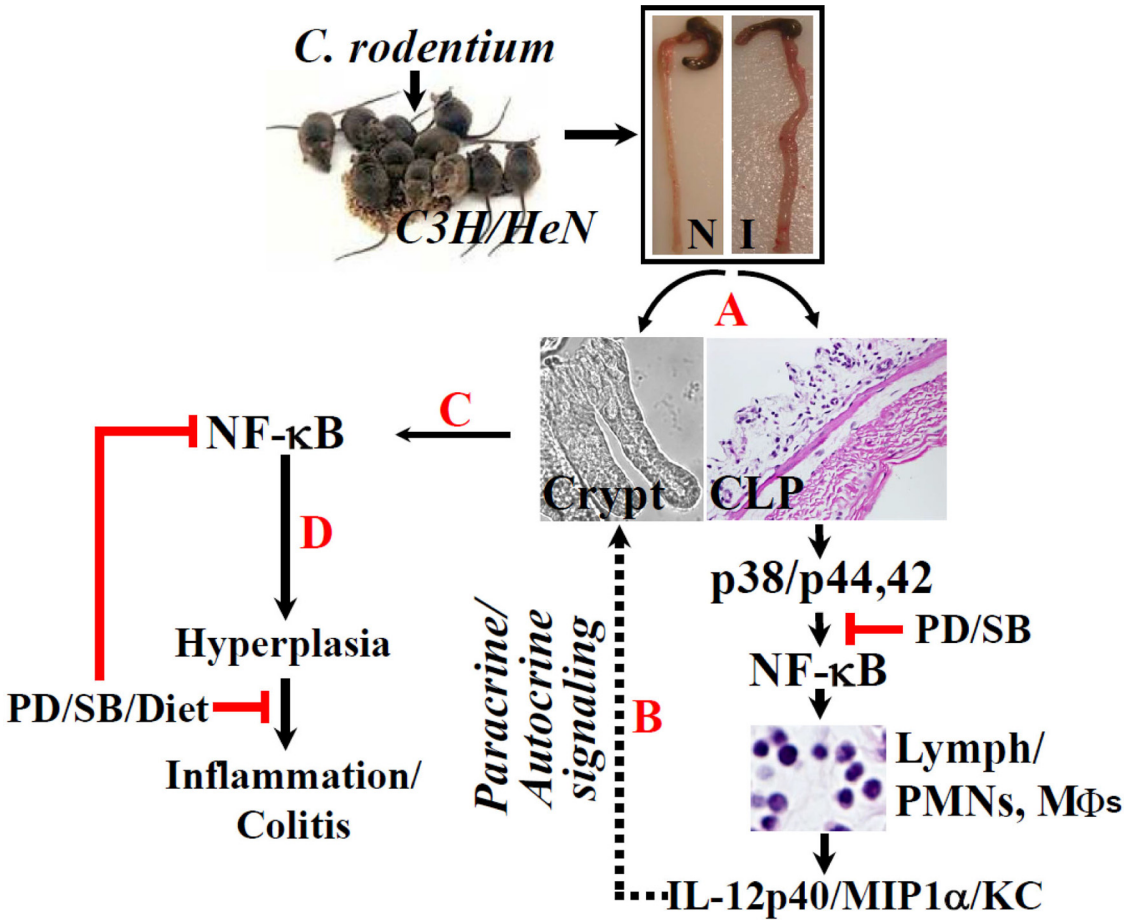

FIG 8 Proposed mechanism of NF-κB's role in hyperplasia and/or inflammation in response to *C. rodentium* infection. Following isolation of crypts and CLP from uninfected (N) or *C. rodentium*-infected (I) distal colons of C3H mice (A), p38 and p44/42 MAPKs may be activated in the CLP, leading to NF-κB-induced recruitment of immune and inflammatory cells in association with release of proinflammatory cytokines/chemokines. This may facilitate NF-κB activation in the crypts (dotted lines; steps B and C), resulting in crypt hyperplasia. The combined paracrine/autocrine effort may eventually prime the mucosa toward inflammation and/or colitis (D). Both p38 (SB203580) and p44/42 (PD98059) inhibitors along with dietary interventions may significantly affect the infection outcome by modulating NF-κB activity in the two compartments.

During the investigation, we discovered that both pectin and the curcumin diet significantly ameliorated colitis by (i) blocking increases in $CD3^+$ T cells, Mϕs, and PMNs (mostly neutrophils), as reflected in a significant reduction in MPO activity in the treated animals, and (ii) by blocking increases in proinflammatory cytokines/chemokines in the treated animals. At the same time, however, both pectin and curcumin promoted crypt hyperplasia and inhibition of apoptosis in the crypts due primarily to a lack of an inhibitory effect on NF-κB activity (Fig. 7). None of these effects was due to interference with the *C. rodentium*'s infection process as the bacterial counts from treated animals were not significantly different from those untreated animals. This apparent paradox not only suggests that both pectin and curcumin are anti-inflammatory but also illustrates a novel observation that they may be proproliferatory, which may facilitate restoration of crypt integrity following an inflammatory insult. Utilizing SAMP1/YitFc (SAMP) mice with chronic Crohn's disease-like ileitis, Pagnini et al. (23) recently showed that pretreatment of SAMP mice with probiotic VSL#3 for 6 weeks before the onset of ileitis prevented the occurrence of intestinal inflammation through a mechanism involving stimulation of TNF-α in the intestinal epithelium and restitution of normal barrier function, suggesting that probiotics promote gut health through stimulation rather than suppression of the innate immune system. In another study, Bhattacharyya et al. (4) showed that curcumin prevented tumor-induced thymic atrophy by restoring NF-κB activity in thymic T cells, suggesting an immunomodulatory role *in vivo*. Since NF-κB is an important component of the epithelial innate immunity, it is tempting to speculate that dietary modulation of its activity in the crypts through pectin, a prebiotic, and curcumin may be associated with promoting the protective immunity and restoring the barrier function, thereby ameliorating colitis in C3H mice. Indeed, we showed in a recently concluded study that both curcumin and an herbal product, *Aegle marmelos*, significantly blocked increases in paracellular permeability and replenished the mucus layer, thereby ameliorating *C. rodentium*/dibenzazepine-induced colitis in NIH/Swiss mice (data not shown). Thus, dietary modulation of NF-κB activity *in vivo* may increase mucosal regeneration following injury to the gut by therapeutically targeting cell death in inflammatory bowel disease in an effort to promote cell survival and favor more effective healing for active inflammation. Figure 8 represents a proposed model depicting the sequence of events related to hyperplasia and/or colitis following *C. rodentium* infection in C3H mice. The TMCH

model therefore offers an excellent template to study mucosal remodeling following bacterial infection.

ACKNOWLEDGMENTS

This work was funded by National Cancer Institute grant R01 CA131413 to S.U. from the U.S. National Institutes of Health and start-up funds from The University of Oklahoma.

REFERENCES

1. **Abraham C, Medzhitov R.** 2011. Interactions between the host innate immune system and microbes in inflammatory bowel disease. Gastroenterology **140**:1729–1737.
2. **Barthold SW, Osbaldiston GW, Jonas AM.** 1977. Dietary, bacterial, and host genetic interactions in the pathogenesis of transmissible murine colonic hyperplasia. Lab. Anim. Sci. **27**:938–945.
3. **Berg DJ, et al.** 1996. Enterocolitis and colon cancer in interleukin-10-deficient mice are associated with aberrant cytokine production and CD4(1) TH1-like responses. J. Clin. Invest. **98**:1010–1020.
4. **Bhattacharyya, S., et al.** 2007. Tumor-induced oxidative stress perturbs nuclear factor-kappaB activity-augmenting tumor necrosis factor-alpha-mediated T-cell death: protection by curcumin. Cancer Res. **67**:362–370.
5. **Bohuslav J, Chen LF, Kwon H, Mu Y, Greene WC.** 2004. p53 induces NF-κB activation by an IκB kinase-independent mechanism involving phosphorylation of p65 by ribosomal S6 kinase 1. J. Biol. Chem. **279**: 26115–26125.
6. **Boquoi A, Jover R, Chen T, Pennings M, Enders GH.** 2009. Transgenic expression of VEGF in intestinal epithelium drives mesenchymal cell interactions and epithelial neoplasia. Gastroenterology **136**:596–606.
7. **Borenshtein D, McBee ME, Schauer DB.** 2008. Utility of the *Citrobacter rodentium* infection model in laboratory mice. Curr. Opin. Gastroenterol. **24**:32–37.
8. **Borenshtein D, Nambiar PR, Groff EB, Fox JG, Schauer DB.** 2007. Development of fatal colitis in FVB mice infected with *Citrobacter rodentium.* Infect. Immun. **75**:3271–3281.
9. **Brown K, Gerstberger S, Carlson L, Franzoso G, Siebenlist U.** 1995. Control of IκB-alpha proteolysis by site-specific, signal-induced phosphorylation. Science **267**:1485–1488.
10. **Bry L, Brigl M, Brenner MB.** 2006. $CD4^+$-T-cell effector functions and costimulatory requirements essential for surviving mucosal infection with *Citrobacter rodentium.* Infect. Immun. **74**:673–681.
11. **Chandrakesan P, et al.** 2010. Novel changes in NF-κB activity during progression and regression phases of hyperplasia: role of MEK, ERK, and p38. J. Biol. Chem. **285**:33485–33498.
12. **Docena G, et al.** 2010. Down-regulation of p38 mitogen-activated protein kinase activation and proinflammatory cytokine production by mitogen-activated protein kinase inhibitors in inflammatory bowel disease. Clin. Exp. Immunol. **162**:108–115.
13. **Doerre S, Corley RB.** 1999. Constitutive nuclear translocation of NF-κB in B cells in the absence of IκB degradation. J. Immunol. **163**:269–277.
14. **Finlay BB, Falkow S.** 1997. Common themes in microbial pathogenicity revisited. Microbiol. Mol. Biol. Rev. **61**:136–169.
15. **Grisham MB, Hernandez LA, Granger DN.** 1986. Xanthine oxidase and neutrophil infiltration in intestinal ischemia. Am. J. Physiol. **251**:G567–G574.
16. **Kang YJ, et al.** 2010. Epithelial p38α controls immune cell recruitment in the colonic mucosa. PLoS Pathog. **6**:e1000934.
17. **Lebeis SL, Bommarius B, Parkos CA, Sherman MA, Kalman D.** 2007. TLR signaling mediated by MyD88 is required for a protective innate immune response by neutrophils to *Citrobacter rodentium.* J. Immunol. **179**:566–577.
18. **Maaser C, et al.** 2001. Colonic epithelial cells induce endothelial cell expression of ICAM-1 and VCAM-1 by a NF-κB-dependent mechanism. Clin. Exp. Immunol. **124**:208–213.
19. **MacDonald TT, Monteleone G.** 2005. Immunity, inflammation and allergy in the gut. Science **307**:1920–1925.
20. **Mizoguchi A, Mizoguchi E.** 2008. Inflammatory bowel disease, past, present and future: lessons from animal models. J. Gastroenterol. **43**:1–17.
21. **Mundy R, MacDonald TT, Dougan G, Frankel G, Wiles S.** 2005. *Citrobacter rodentium* of mice and man. Cell Microbiol. **7**:1697–1706.
22. **Neurath MF, Pettersson S, Meyer zum Buschenfelde KH, Strober W.** 1996. Local administration of antisense phosphorothioate oligonucleotides to the p65 subunit of NF-κB abrogates established experimental colitis in mice. Nat. Med. **2**:998–1004.
23. **Pagnini C, et al.** 2010. Probiotics promote gut health through stimulation of epithelial innate immunity. Proc. Natl. Acad. Sci. U. S. A. **107**:454–459.
24. **Peluso I, Pallone F, Monteleone G.** 2006. Interleukin-12 and Th1 immune response in Crohn's disease: pathogenetic relevance and therapeutic implication. World J. Gastroenterol. **12**:5606–5610.
25. **Seidelin JB.** 2004. Colonic epithelial cell turnover: possible implications for ulcerative colitis and cancer initiation. Scand. J. Gastroenterol. **39**:201–211.
26. **Sellin JH, Wang Y, Singh P, Umar S.** 2009. Beta-Catenin stabilization imparts crypt progenitor phenotype to hyperproliferating colonic epithelia. Exp. Cell Res. **315**:97–109.
27. **Shibata W, et al.** 2007. The IκB kinase (IKK) inhibitor, NEMO-binding domain peptide, blocks inflammatory injury in murine colitis. J. Immunol. **179**:2681–2685.
28. **Smythies LE, et al.** 2005. Human intestinal macrophages display profound inflammatory anergy despite avid phagocytic and bacteriocidal activity. J. Clin. Invest. **115**:66–75.
29. **Umar S, Morris AP, Kourouma F, Sellin JH.** 2003. Dietary pectin and calcium inhibit colonic proliferation in vivo by differing mechanisms. Cell Prolif. **36**:361–375.
30. **Umar S, Sellin JH, Morris AP.** 2000. Increased nuclear translocation of catalytically active PKC-zeta during mouse colonocyte hyperproliferation. Am. J. Physiol. Gastrointest. Liver Physiol. **279**:G223–237.
31. **Umar S, Scott J, Sellin JH, Dubinsky WP, Morris AP.** 2000. Murine colonic mucosa hyperproliferation. I. Elevated CFTR expression and enhanced cAMP-dependent Cl(−) secretion. Am. J. Physiol. Gastrointest. Liver Physiol. **278**:G753–G764.
32. **Umar S, Sarkar S, Cowey S, Singh P.** 2008. Activation of NF-kappaB is required for mediating proliferative and antiapoptotic effects of progastrin on proximal colonic crypts of mice, in vivo. Oncogene **27**:5599–5611.
33. **Umar S, Sarkar S, Wang Y, Singh P.** 2009. Functional cross-talk between beta-catenin and NFκB signaling pathways in colonic crypts of mice in response to progastrin. J. Biol. Chem. **284**:22274–22284.
34. **Umar S, Wang Y, Morris AP, Sellin JH.** 2007. Dual alterations in casein kinase I-epsilon and GSK-3β modulate beta-catenin stability in hyperproliferating colonic epithelia. Am. J. Physiol. Gastrointest. Liver Physiol. **292**:G599–G607.
35. **Umar S, Wang Y, Sellin JH.** 2005. Epithelial proliferation induces novel changes in APC expression. Oncogene **24**:6709–6718.
36. **Vallance BA, Deng W, Jacobson K, Finlay BB.** 2003. Host susceptibility to the attaching and effacing bacterial pathogen *Citrobacter rodentium.* Infect. Immun. **71**:3443–3453.
37. **Waetzig GH, Seegert D, Rosenstiel P, Nikolaus S, Schreiber S.** 2002. p38 mitogen-activated protein kinase is activated and linked to TNF-alpha signaling in inflammatory bowel disease. J. Immunol. **168**:5342–5351.
38. **Wang Y, Xiang GS, Kourouma F, Umar S.** 2006. *Citrobacter rodentium*-induced NF-kappaB activation in hyperproliferating colonic epithelia: role of p65 (Ser536) phosphorylation. Br. J. Pharmacol. **148**:814–824.
39. **Zhong H, SuYang H, Erdjument-Bromage H, Tempst P, Ghosh S.** 1997. The transcriptional activity of NF-κB is regulated by the IκB-associated PKAc subunit through a cyclic AMP-independent mechanism. Cell **89**: 413–424.